

Yiheng Xue

International Center for Applied Mechanics;
State Key Laboratory for Strength and Vibration of
Mechanical Structures,
Xi'an Jiaotong University,
No. 28, West Xianning Road,
Xi'an, Shaanxi 710049, China
e-mail: yihengxue@stu.xjtu.edu.cn

Zidi Zhou

International Center for Applied Mechanics;
State Key Laboratory for Strength and Vibration of
Mechanical Structures,
Xi'an Jiaotong University,
No. 28, West Xianning Road,
Xi'an, Shaanxi 710049, China
e-mail: zhouzidi@stu.xjtu.edu.cn

Jincheng Lei

International Center for Applied Mechanics;
State Key Laboratory for Strength and Vibration of
Mechanical Structures,
Xi'an Jiaotong University,
No. 28, West Xianning Road,
Xi'an, Shaanxi 710049, China
e-mail: jinchenglei@xjtu.edu.cn

Zishun Liu¹

Mem. ASME

International Center for Applied Mechanics;
State Key Laboratory for Strength and Vibration of
Mechanical Structures,
Xi'an Jiaotong University,
No. 28, West Xianning Road,
Xi'an, Shaanxi 710049, China
e-mail: zishunliu@mail.xjtu.edu.cn

A Constitutive Model of Water-Triggered Shape Memory Hydrogels and Its Finite Element Implementation

Shape memory hydrogel is a type of hydrogel whose shape can transform between a temporary shape and its initial shape when exposed to external stimuli, such as water, temperature, and pH. Over the last decade, shape memory hydrogels have gained increasing interest owing to their distinct properties; however, constitutive models to describe their shape memory mechanism are still lacking. In this paper, we propose a constitutive model for water-triggered shape memory hydrogels based on the transition between the sparse and dense phases. In the model, the shape memory process is identified using two internal variables: the frozen deformation gradient and dense phase volume fraction. To validate the model for describing shape memory effects, we implemented the model in the finite element method using a user-defined element (UEL) subroutine in ABAQUS. To verify the accuracy of the proposed UEL, we simulated the water-triggered shape memory effects in different recovery processes under different uniaxial loads. Furthermore, we investigated the water-triggered shape memory behavior of a self-bending bilayer structure and a four-arm gripper structure using both experiments and simulations. Good agreement was observed between the simulation and experimental results.

[DOI: 10.1115/1.4056912]

Keywords: water-triggered, shape memory hydrogels, constitutive model, finite-element implementation, constitutive modeling of materials, mechanical properties of materials

1 Introduction

Hydrogels are polymers consisting of a three-dimensional hydrophilic polymer network and a large amount of water. Hydrogels that possess shape memory effects (SMEs), called shape memory hydrogels (SMHs), have attracted increasing interest in recent years. The SMH can maintain a temporary shape and recover to its initial shape under external environmental stimuli, such as water [1–6], temperature [7,8], pH [9,10], and ion concentration [11–14]. Compared with the low reversible strain (<1000%) of traditional shape memory polymers, SMHs exhibit a much higher reversible strain, exceeding 2600% [15]. In addition, SMHs have many advantages, such as biocompatibility, self-healing, lightweight, and multi-stimuli responsive capabilities [12,16,17]. Owing to these distinguishing characteristics, SMHs have promising applications in many fields, such as drug delivery, actuator, soft robots, and energy storage [8,10–12,17–21].

To satisfy the increasing interest in the application of SMHs, a constitutive model that can properly describe its shape memory mechanism is imperative. Recently, constitutive models have been established for temperature-triggered SMHs. Chen et al. [22] developed a hyper-elastic model for double-network SMHs triggered by temperature. This model can accurately describe the

stress responses of the hydrogel in hot and cold states. To investigate the change in the stored strain during shape recovery process, Lu et al. [23] formulated a thermodynamic model for the cooling-triggered shape memory effects of a double-network hydrogel. The good agreement between the analytical and experimental results indicates that the model can capture the evolution of the stored strain when immersing the hydrogel with a temporary shape in cooling water. For SMHs triggered by a thermal stimuli, such as water, a corresponding constitutive model is still lacking. Therefore, a new constitutive model for SMHs triggered by other stimuli should be developed.

Over the past decades, several constitutive models have been established based on viscoelasticity and phase transition to describe the shape memory behaviors of shape memory polymers [24–26]. Viscoelastic constitutive models utilize rheological elements composed of dashpot, spring, and frictional elements to evaluate the thermomechanical properties of shape memory polymers [27,28]. Different from the viscoelastic methods, phase transition models phenomenologically describe shape memory behaviors based on the assumption that the shape memory polymer is a mixture of hard phase and active phase [29,30]. In these models, shape memory effects are triggered by the change in temperature. Moreover, thermal strain is often neglected because its value is much smaller than mechanical strain. Different from shape memory polymers, the swelling strain of shape memory hydrogels induced by other stimuli, such as water and pH, should be considered because the swelling strain can reach up to 100%, as reported in Ref. [1]. To model the swelling strain of hydrogels, many researchers have developed constitutive models based on the Flory–Rehner

¹Corresponding author.

Contributed by the Applied Mechanics Division of ASME for publication in the JOURNAL OF APPLIED MECHANICS. Manuscript received January 17, 2023; final manuscript received February 12, 2023; published online March 16, 2023. Assoc. Editor: Pradeep Sharma.

free-energy theory [31,32]. In this study, inspired by the phase transition theory of shape memory polymers and the Flory–Rehner free-energy theory of hydrogels, we investigated the mechanical properties of water-triggered shape memory hydrogels.

In order to apply the constitutive model to investigate the mechanical behaviors of complex structures, the constitutive model should be developed using the finite element method (FEM). To date, several researchers have developed user subroutines provided by the commercial finite element software ABAQUS to implement the constitutive model in FEM. Hong et al. [31] used UHYPER to implement an equilibrium state of a gel under chemical and mechanical loads. To enhance the robustness of the algorithm, a thermomechanical model for temperature-sensitive hydrogels was implemented in UMAT [32], in which the user-defined stress and corresponding stiffness matrix should be specified. Meanwhile, a numerical approximation of the tangent moduli was proposed by Miehe [33] and further developed by Sun et al. [34] by perturbing the deformation gradient and material matrix. However, for SMHs, the proposed subroutines UHYPER and UMAT cannot be used to address coupling field problems. To simulate the large deformation of hydrogels under multiple fields, Chester et al. [35] presented a FEM using the user-defined element (UEL) subroutine by providing additional degrees-of-freedom at each node. Recently, several multi-field coupling problems have been studied using the FEM based on Chester's work [36,37]. However, no study has been conducted on the fully coupled shape memory theory and numerical implementation of SMHs.

In this study, a constitutive model characterizing the water-triggered shape memory process of hydrogels was developed and implemented using UEL in ABAQUS. The remainder of this paper is organized as follows. Section 2 presents the proposed constitutive model, which includes the internal state variables in the phase transition process and free-energy function for water-triggered SMHs. The implementation of the proposed model using FEM is discussed in Sec. 3. Section 4 presents a validation of the model. Concluding remarks are provided in Sec. 5.

2 Constitutive Model for Water-Triggered Shape Memory Hydrogels

2.1 Phase Transition and Internal State Variables. In the water-triggered shape memory process, the shape programmed at a high water content can be maintained when the hydrogel is dehydrated to a low water content under constraint, and the initial shape can be recovered after hydrating the temporary shape of the hydrogel to a high water content. During this process, the polymer networks of the hydrogel exhibit different states under different water contents. For hydrogels with high water content, the polymer networks exhibit a sparse domain because of the large amount of free water distributed around them. As the hydrogel is dehydrated, the free water is lost and the bound water remains, which results in the polymer networks exhibiting a dense domain. Therefore, we assume that hydrogel with high water content is primarily in the sparse phase and hydrogel with low water content is primarily in the dense phase. The terms “dense” and “sparse” are used to refer to states of the polymer networks in low and high water content, respectively. In this paper, we consider hydrogel is a mixture of two types of extreme phases in different water content: the “dense phase” and “sparse phase.” As the hydrogel dehydrating, the sparse phase gradually transforms into the dense phase, and vice versa. Additionally, we named this process the phase transition in hydrogels.

To describe the storage and release of the programmed deformation during the phase transition, the frozen deformation gradient F_f in the dense phase is proposed as an internal state variable. In Fig. 1, a typical water-triggered shape memory process is described. The hydrogel is applied on a mechanical load F_s while the hydrogel is in the sparse phase. As the water content decreases, the sparse

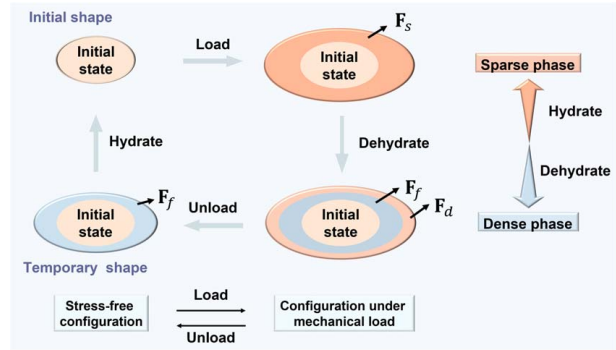


Fig. 1 Schematic of a typical water-triggered shape memory process. F_s and F_d denote the elastic deformation gradient of sparse and dense phases, respectively; F_f denotes the frozen deformation gradient.

phase undergoes phase transition and transforms into the dense phase. Meanwhile, most of the pre-deformation locks in the dense phase during the phase transition under constraint, and F_f is used to denote the frozen deformation. The residual elastic deformation in the dense phase is denoted by F_d . When the hydrogel undergoes unloading at low water content, the elastic deformation F_d in the dense phase is released, and the frozen deformation F_f is retained. As the hydrogel is hydrated to a high water content, the frozen deformation F_f is released, and the temporary shape is recovered to its initial shape. According to the above analysis, the relationship between the deformation gradients in the two phases is expressed as

$$F = F_s = F_d F_f \quad (1)$$

where F denotes the mapping of material coordinates from the reference state to the current state. To elucidate such shape memory effects in the phase transition process, we propose an evolution model for the frozen deformation gradient F_f in the shape memory process, that is

$$F_f = \begin{cases} I, & \text{initial value} \\ l \left(\frac{F}{\lambda_s} - I \right) + I, & \dot{\mu} < 0 \\ \text{unchanged}, & \dot{\mu} \geq 0 \end{cases} \quad (2)$$

where l is a parameter that denotes the degree of the deformation storage, λ_s is the free-swelling stretch relative to the dry polymer state at the corresponding chemical potential, $\dot{\mu}$ is the rate of change of the chemical potential, $\dot{\mu} < 0$ is the dehydrating process, and $\dot{\mu} > 0$ is the hydrating process. In the initial state, the frozen deformation gradient is assumed to be a unit tensor, because there is no frozen deformation. In the constraint-dehydrate process, i.e., $\dot{\mu} < 0$, frozen deformation is supposed to be related to the deformation gradient in the current state in Eq. (2). As a result, the programmed deformation can be stored in F_f after dehydration under constraints. In the hydration process, i.e., $\dot{\mu} > 0$, the frozen deformation in the dense phase is assumed to be constant. Frozen deformation in the dense phase is released as the dense phase transforms into a sparse phase. Consequently, when the hydrogel completely transforms from the dense phase to the sparse phase, the frozen deformation can be totally released after hydration.

To quantify the degree of the phase transition, the volume fractions of dense phase and sparse phase in hydrogel are defined as ϕ_d and ϕ_s , respectively, and $\phi_d + \phi_s = 1$. As mentioned earlier, the hydrogel with high water content is primarily in the sparse phase. Hence, the volume fraction of the sparse phase in this state equals one, i.e., $\phi_s = 1$, and the volume fraction of the dense phase in this state equals zero, i.e., $\phi_d = 0$. In this paper, we assume that the volume fractions of two phases are related to the normalized chemical potential $\hat{\mu}$ and specify that the range of the chemical potential of the shape memory process occurs from $\hat{\mu}_l$ to $\hat{\mu}_h$. The normalized chemical

potential $\hat{\mu}$ is equal to μ/kT , which is detailed in Sec. 2.3. According to the assumption of the phase transition, we can obtain the boundary value of ϕ_d , $\phi_d(\hat{\mu}_l) = 1$ and $\phi_d(\hat{\mu}_h) = 0$. Similar to the phase volume fraction in shape memory polymers [38], we assume that the volume fraction of dense phase ϕ_d is

$$\phi_d(\hat{\mu}) = 1 - \frac{1}{1 + \exp\left(-\frac{\hat{\mu} - \hat{\mu}_r}{A}\right)} \quad (3)$$

where A is a parameter that characterizes the width of the phase transition zone, and $\hat{\mu}_r$ is the reference chemical potential at the phase transformation center (as shown in Fig. 2). In Eq. (3), the dense phase volume fraction ϕ_d is approximately equal to zero at a high chemical potential $\hat{\mu}_h$; i.e., the gel is entirely in the sparse phase. In contrast, at a low chemical potential, $\hat{\mu}_l$, ϕ_d is approximately equal to one; i.e., the gel is in the dense phase (Fig. 2).

2.2 Constitutive Equation. We use the total deformation gradient of the polymer network \mathbf{F} and the chemical potential of the solvent μ in the current state as two independent variables for water-triggered SMHs. First, the free energy $W(\mathbf{F}, C)$, which is a function of the total deformation gradient \mathbf{F} and the water concentration C , is developed. Subsequently, free energy $\hat{W}(\mathbf{F}, \mu)$ which is related to the total deformation gradient \mathbf{F} and the chemical potential μ is further derived.

According to the constitutive framework for neutral gels [39], the free energy function of the shape memory hydrogels is assumed to be the sum of two parts

$$W(\mathbf{F}, C) = W_{stretch} + W_{mix} \quad (4)$$

where $W_{stretch}$ is the energy due to the stretching of the polymer networks, and W_{mix} is the energy due to the mixing of water and polymer networks.

To describe the evolution of the stretching free energy during the phase transition process, we divide the stretching free energy of the polymer networks into the sum of the free energies of the two phases, that is

$$W_{stretch} = \phi_d W_d + \phi_s W_s \quad (5)$$

where W_d and W_s denote the free energies of the dense and sparse phases, respectively. The objective of this paper is to demonstrate the modeling of shape memory effects in hydrogels, rather than investigating alternative forms of hyper-elastic materials. Here, we adopt the well-known free-energy function to describe the

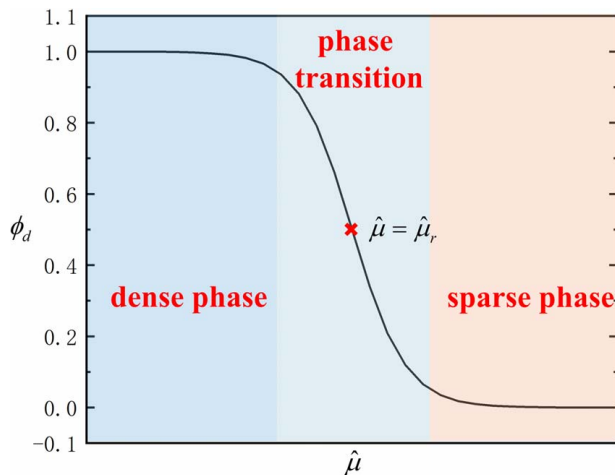


Fig. 2 Relationship between the dense volume fraction ϕ_d and normalized chemical potential $\hat{\mu}$; $\hat{\mu}_r$ denotes the reference normalized chemical potential at the phase transformation center

stretching of free energies, that is

$$W_d = \frac{G_d}{2} (I_{1d} - 3 - 2 \log J_d) \quad (6)$$

in the dense phase, and

$$W_s = \frac{G_s}{2} (I_{1s} - 3 - 2 \log J_s) \quad (7)$$

in the sparse phase, where G_d and G_s denote the shear moduli of the dense and sparse phases, respectively. $I_{1d} = \text{tr}(\mathbf{F}_d^T \mathbf{F}_d)$, $I_{1s} = \text{tr}(\mathbf{F}_s^T \mathbf{F}_s)$, $J_d = \det(\mathbf{F}_d)$ and $J_s = \det(\mathbf{F}_s)$. In this paper, we assume that the shear modulus of the sparse phase is

$$G_s = NkT \quad (8)$$

where N is the number of polymeric chains per reference volume, k is the Boltzmann constant, and T is the absolute temperature.

For the mixing free energy of the hydrogel, a general form [40,41] is taken as

$$W_{mix} = -\frac{kT}{v} \left(\nu C \log \left(1 + \frac{1}{\nu C} \right) + \frac{\chi}{1 + \nu C} \right) \quad (9)$$

where χ is a dimensionless measure of the enthalpy of mixing and v is the volume per solvent molecule.

In our model, the chemical potential of the water μ is used to investigate the change in water content, which is the conjugate variable of the concentration of the water C . The chemical potential is equal to the derivative of the free energy with respect to C , i.e.

$$\mu = \frac{\partial W}{\partial C} \quad (10)$$

Utilizing Legendre transformation and Eq. (10), a new free-energy function \hat{W} related to the deformation and chemical potential is introduced:

$$\hat{W}(\mathbf{F}, \mu) = W(\mathbf{F}, C) - \mu C \quad (11)$$

Considering that all molecules in the gel are incompressible, the volume of the gel is equal to the sum of the volumes of the dry network and solvent, i.e., $J = 1 + \nu C$, and $J = \det \mathbf{F}$. Subsequently, by substituting Eqs. (4)–(9) into Eq. (11), the free-energy function with respect to the deformation gradient and chemical potential can be obtained

$$\begin{aligned} \hat{W}(\mathbf{F}, \mu) = & \frac{\phi_d G_d}{2} (I_{1d} - 3 - 2 \log J_d) \\ & + \frac{\phi_s NkT}{2} (I_{1s} - 3 - 2 \log J_s) \\ & - \frac{kT}{v} \left((J - 1) \log \left(\frac{J}{J - 1} \right) + \frac{\chi}{J} \right) - \frac{\mu}{v} (J - 1) \end{aligned} \quad (12)$$

The Cauchy stress σ is defined as

$$\sigma = \frac{1}{J} \frac{\partial \hat{W}}{\partial \mathbf{F}} \cdot \mathbf{F}^T \quad (13)$$

Substituting Eq. (12) into Eq. (13), the constitutive relationship related to the total deformation gradient \mathbf{F} and chemical potential of the solvent μ can be expressed as

$$\begin{aligned} \frac{\sigma v}{kT}(\mathbf{F}, \mu) = & \frac{\phi_d G_d v}{JkT} (\mathbf{B}_d - \mathbf{I}) + \frac{\phi_s N v}{J} (\mathbf{B}_s - \mathbf{I}) \\ & + \left(\log \left(1 - \frac{1}{J} \right) + \frac{1}{J} + \frac{\chi}{J^2} - \frac{\mu}{kT} \right) \mathbf{I} \end{aligned} \quad (14)$$

where \mathbf{B}_d and \mathbf{B}_s are the left Cauchy-Green deformation tensors of \mathbf{F}_d and \mathbf{F}_s , respectively, and \mathbf{I} is the second-order unit tensor. To simplify the calculation process, we normalize the stress by kT/v , and normalize the chemical potential by kT , i.e., $\hat{\mu} = \mu/kT$. At

room temperature (25 °C), $kT/v = 4 \times 10^7$ Pa. To determine the frozen deformation gradient in Eq. (11), the free-swelling stretch λ_s can be obtained from Eq. (14) under a free-swelling process. In a free-swelling process of a gel, $\mathbf{F} = \lambda_s \mathbf{I}$, and the corresponding stress is equal to zero. By setting the stress in Eq. (14) to zero, the relationship between the swelling stretch λ_s and the corresponding chemical potential μ_s can be obtained

$$\phi_d G_d (\lambda_s^2 - 1) + \phi_s N k T (\lambda_s^2 - 1) + \lambda_s^3 \log \left(1 - \frac{1}{\lambda_s^3} \right) + 1 + \frac{\chi}{\lambda_s^3} - \frac{\mu_s}{v} \lambda_s^3 = 0 \quad (15)$$

Using Eq. (15), we can derive the free-swelling stretch at any given chemical potential and determine the corresponding frozen deformation gradient in Eq. (2). Together with Eqs. (1)–(3), the constitutive relationship in Eq. (14) can be used to describe the shape memory behaviors of water-triggered SMHs.

3 Finite-Element Implementation

To utilize the proposed model to predict the water-triggered shape memory behavior of hydrogels with complex deformations, we require a finite-element implementation. Because of the strong coupling between the deformation field and chemical potential field, the UHYPER and UMAT adopted in previous studies are not applicable to the proposed model. Different from UHYPER and UMAT, the UEL is suitable for solving multi-field coupling problems because it provides additional degrees-of-freedom available for other physical fields. Therefore, the UEL is adopted to implement the proposed constitutive model into FEM to investigate the performance of the model on the description of water-triggered shape memory behaviors by writing a 3D eight-node linear isoparametric element denoted as U3D8.

3.1 Decomposition of Deformation Gradient in Finite Element Model Procedure. To achieve the water-triggered shape memory effects of the proposed model, the deformation gradient is decomposed in the FEM procedure. First, the deformation gradient is decomposed by changing the reference configuration to a swollen state owing to the singular problem in the dry state of the hydrogel. Subsequently, the deformation gradient is further decomposed to separate the swelling stretch and mechanical stretch in the FEM procedure.

The reference state of the proposed model is the dry polymer network; thus, the constitutive relationship in Eq. (14) is singular when the hydrogel contains no water, i.e., $J = 1$. Here, we select an initial free-swelling condition as a new reference state for the finite-element implementation

$$\mathbf{F}_0 = \begin{bmatrix} \lambda_0 & & \\ & \lambda_0 & \\ & & \lambda_0 \end{bmatrix} \quad (16)$$

where λ_0 is an isotropic swelling stretch relative to a dry network, which can be obtained using Eq. (15) when given an initial chemical potential μ_0 . Hence, the current deformation of the gel \mathbf{F}' can be expressed as $\mathbf{F}' = \mathbf{F} \mathbf{F}_0^{-1}$. The actual volume ratio can be expressed as $J = \lambda_0^3 J'$, where J' is the determinant of the current deformation gradient. Therefore, the true stress with respect to \mathbf{F}' and μ is further derived as

$$\frac{\sigma v}{kT}(\mathbf{F}', \mu) = \frac{\phi_d G_d v}{J' k T} \left(\frac{\mathbf{B}'_d}{\lambda_0} - \frac{\mathbf{I}}{\lambda_0^3} \right) + \frac{\phi_s N v}{J'} \left(\frac{\mathbf{B}'_s}{\lambda_0} - \frac{\mathbf{I}}{\lambda_0^3} \right) + \left(\log \left(1 - \frac{1}{J' \lambda_0^3} \right) + \frac{1}{J' \lambda_0^3} + \frac{\chi}{J'^2 \lambda_0^6} - \frac{\mu}{kT} \right) \mathbf{I} \quad (17)$$

where $\mathbf{B}'_d = \mathbf{F}'_d \mathbf{F}'_d{}^T$, $\mathbf{B}'_s = \mathbf{F}'_s \mathbf{F}'_s{}^T$, and $\mathbf{F}'_d = \mathbf{F}' \mathbf{F}'_f^{-1}$, $\mathbf{F}'_s = \mathbf{F}'$.

In our defined element, the nodal displacement field is influenced in two forms, one is the isotropic volume change caused by the chemical potential load and the other is the displacement that depends on the mechanical load. In the numerical implementation procedure, it is difficult to capture the swelling deformation when the initial state is swollen [35]. To solve this problem, we separate the displacements caused by isotropic swelling deformation before calculating the residual vectors and corresponding tangents. This operation is performed by dividing \mathbf{F}' by swollen stretch

$$\mathbf{F}'' = \frac{\mathbf{F}'}{\lambda_w} \quad (18)$$

where λ_w is the swelling or deswelling stretch relative to the initial state at chemical potential μ_s , and $\lambda_w = \lambda_s / \lambda_0$. The decomposed deformation gradient \mathbf{F}'' denotes the mechanical deformation gradient, which means that \mathbf{F}'' is related only to the displacement caused by the mechanical load. Substituting Eq. (18) into Eq. (17), the true stress in calculating the residual vector is expressed as a function of \mathbf{F}'' as follows:

$$\frac{\sigma v}{kT}(\mathbf{F}'', \mu) = \frac{\phi_d G_d v}{J'' k T} \left(\frac{\mathbf{B}''_d}{\lambda_s} - \frac{\mathbf{I}}{\lambda_s^3} \right) + \frac{\phi_s N v}{J''} \left(\frac{\mathbf{B}''_s}{\lambda_s} - \frac{\mathbf{I}}{\lambda_s^3} \right) + \left(\log \left(1 - \frac{1}{J'' \lambda_s^3} \right) + \frac{1}{J'' \lambda_s^3} + \frac{\chi}{J''^2 \lambda_s^6} - \frac{\mu}{kT} \right) \mathbf{I} \quad (19)$$

where $\mathbf{B}''_d = \mathbf{F}''_d \mathbf{F}''_d{}^T$, $\mathbf{B}''_s = \mathbf{F}''_s \mathbf{F}''_s{}^T$, and $\mathbf{F}''_d = \mathbf{F}'' \mathbf{F}_f^{-1}$, $\mathbf{F}''_s = \mathbf{F}''$. Frozen deformation gradient \mathbf{F}_f in Eq. (2) is further derived in relation to \mathbf{F}'' as follows:

$$\mathbf{F}_f = \begin{cases} \mathbf{I}, & \text{initial value} \\ l(\mathbf{F}'' - \mathbf{I}) + \mathbf{I}, & \mu < 0 \\ \text{unchanged}, & \mu \geq 0 \end{cases} \quad (20)$$

3.2 Implementation in User-Defined Element. Here, the residual vectors and the corresponding tangents matrix to be defined in the UEL are derived in detail. Each node of the element has four degrees-of-freedom: the first three are the displacements in three directions in the global coordinate system, and the fourth is the chemical potential. The UEL solves the coupled equations of a use-defined element using a Newton procedure by calculating the following residuals of the displacement and chemical potential, respectively,

$$\begin{cases} (\mathbf{R}_u)^i = -\int_{B'} \sigma \frac{\partial N^i}{\partial \mathbf{x}} dv \\ (\mathbf{R}_\mu)^j = 0 \end{cases} \quad (21)$$

where i denotes the node index of the element, N^i denotes the corresponding shape function, and dv is an element of the volume in the current configuration. Here, the diffusion of the chemical potential is not considered; thus, the residual vector of the chemical potential \mathbf{R}_μ vanishes. In addition to the residual vectors, the tangents of the residuals with respect to the displacement and chemical potential are required for the UEL subroutine

$$\begin{cases} \mathbf{K}_{uu} = -\frac{\partial \mathbf{R}_u}{\partial \mathbf{u}} \\ \mathbf{K}_{u\mu} = -\frac{\partial \mathbf{R}_u}{\partial \mu} \\ \mathbf{K}_{\mu\mu} = -\frac{\partial \mathbf{R}_\mu}{\partial \mu} \\ \mathbf{K}_{\mu u} = -\frac{\partial \mathbf{R}_\mu}{\partial \mathbf{u}} \end{cases} \quad (22)$$

where \mathbf{u} is the displacement vector of nodes in a finite element. The tangents $\mathbf{K}_{\mu\mu}$ and $\mathbf{K}_{\mu u}$ vanish due to the vanished residual vector \mathbf{R}_μ .

Then, \mathbf{K}_{uu} and $\mathbf{K}_{\mu\mu}$ can be further expressed as [35],

$$\begin{cases} K_{u_i u_k}^{AB} = \int_{B^e} \frac{\partial N^A}{\partial x_j} (\mathbf{D}_{ijkl}) \frac{\partial N^B}{\partial x_l} dv \\ K_{u_i \mu}^{AB} = \int_{B^e} \frac{\partial N^A}{\partial x_i} \left(\frac{\partial \sigma_{ij}}{\partial \mu} \right) \frac{\partial N^B}{\partial x_l} dv \end{cases} \quad (23)$$

where the spatial tangent modulus \mathbf{D} is defined as

$$\mathbf{D}_{ijkl} \stackrel{\text{def}}{=} J''^{-1} F''_{jm} F''_{ln} (\mathbf{D}_p)_{imkn} \quad (24)$$

\mathbf{D}_p is a fourth-order tensor that refers to the tangent stiffness matrix of the first Piola–Kirchhoff stress \mathbf{P} , i.e., $\mathbf{D}_p = \partial \mathbf{P} / \partial \mathbf{F}''$, where $\mathbf{P} = J'' \boldsymbol{\sigma} \mathbf{F}''^{-T}$.

Considering the true stress in Eq. (19), the tangents of the residuals in Eq. (23) can be derived. Equation (20) indicates the partial derivative of \mathbf{F}_f with respect to \mathbf{F}'' is in different forms under different conditions. Therefore, the tangents of the residuals are closely related to the chemical potential conditions.

According to Eq. (20), the derivative of the frozen deformation gradient \mathbf{F}_f with respect to \mathbf{F}'' is

$$\left(\frac{\partial \mathbf{F}_f}{\partial \mathbf{F}''} \right)_{ijkl} = \begin{cases} 0 & , \text{ other condition} \\ l(\mathbf{II})_{ijkl} & , \dot{\mu} < 0 \end{cases} \quad (25)$$

Subsequently, the first Piola–Kirchhoff stress is divided into two parts: the first part \mathbf{P}_1 is related to the frozen deformation gradient \mathbf{F}_f , and the second part \mathbf{P}_2 is independent of \mathbf{F}_f , that is

$$\frac{\mathbf{P}_v}{kT} = \underbrace{\frac{\phi_d G_d v}{kT} \left(\frac{\mathbf{F}'' \mathbf{F}_f^{-1} \mathbf{F}_f^{-T}}{\lambda_s} - \frac{\mathbf{F}''^{-T}}{\lambda_s^3} \right)}_{\mathbf{P}_1} + \underbrace{\phi_s N_v \left(\frac{\mathbf{F}''}{\lambda_s} - \frac{\mathbf{F}''^{-T}}{\lambda_s^3} \right) + \left(J'' \log \left(1 - \frac{1}{J'' \lambda_s^3} \right) + \frac{1}{\lambda_s^3} + \frac{\chi}{J'' \lambda_s^6} - \frac{\mu}{kT} J'' \right) \mathbf{F}''^{-T}}_{\mathbf{P}_2} \quad (26)$$

The tangent stiffness matrix \mathbf{D}_p of the first Piola–Kirchhoff stress \mathbf{P} is expressed as

$$\mathbf{D}_p = \mathbf{D}_{p_1} + \mathbf{D}_{p_2} \quad (27)$$

where \mathbf{D}_{p_1} and \mathbf{D}_{p_2} are the corresponding tangent stiffness matrix of \mathbf{P}_1 and \mathbf{P}_2 , respectively. Hence,

$$\mathbf{D}_{p_1} = \frac{\partial \mathbf{P}_1}{\partial \mathbf{F}''} = \frac{\phi_d G_d v}{kT} \left(\frac{\mathbf{H} \mathbf{F}_f^{-1} \mathbf{F}_f^{-T}}{\lambda_s} + \frac{\mathbf{F}''}{\lambda_s} \frac{\partial (\mathbf{F}_f^{-1})}{\partial \mathbf{F}''} \mathbf{F}_f^{-T} + \frac{\mathbf{F}'' \mathbf{F}_f^{-1} \partial (\mathbf{F}_f^{-T})}{\lambda_s \partial \mathbf{F}''} - \frac{1}{\lambda_s^3} \frac{\partial (\mathbf{F}''^{-T})}{\partial \mathbf{F}''} \right) \quad (28)$$

and

$$\begin{aligned} \mathbf{D}_{p_2} &= \frac{\partial \mathbf{P}_2}{\partial \mathbf{F}''} \\ &= \phi_s N_v \left(\frac{\mathbf{H}}{\lambda_s} - \frac{1}{\lambda_s^3} \frac{\partial (\mathbf{F}''^{-T})}{\partial \mathbf{F}''} \right) \\ &\quad + \left(J'' \log \left(1 - \frac{1}{J'' \lambda_s^3} \right) + \frac{1}{\lambda_s^3} + \frac{\chi}{J'' \lambda_s^6} - \frac{\mu}{kT} J'' \right) \frac{\partial (\mathbf{F}''^{-T})}{\partial \mathbf{F}''} \\ &\quad + \left(\log \left(1 - \frac{1}{J'' \lambda_s^3} \right) + \frac{1}{J'' \lambda_s^3} - \frac{\chi}{J''^2 \lambda_s^6} - \frac{\mu}{kT} \right) \mathbf{F}''^{-T} \frac{\partial J''}{\partial \mathbf{F}''} \end{aligned} \quad (29)$$

where the standard tensor derivatives are described as follows:

$$\begin{aligned} (\mathbf{II})_{ijkl} &= \delta_{ik} \delta_{jl} \cdot \left(\frac{\partial (\mathbf{F}''^{-T})}{\partial \mathbf{F}''} \right)_{ijkl} = -F''_{li}^{-1} F''_{jk}^{-1} \cdot \left(\frac{\partial J''}{\partial \mathbf{F}''} \right)_{ijkl} = J'' F''_{lk}^{-1} \end{aligned} \quad (30)$$

The derivative of \mathbf{F}_f^{-1} with respect to \mathbf{F}'' can be obtained using the chain rule, that is

$$\frac{\partial (\mathbf{F}_f^{-1})}{\partial \mathbf{F}''} = \frac{\partial (\mathbf{F}_f^{-1})}{\partial \mathbf{F}_f} \frac{\partial \mathbf{F}_f}{\partial \mathbf{F}''} \quad (31)$$

Combining the Eqs. (26)–(31), tangent stiffness matrix \mathbf{D}_p in Eq. (27) can be fully determined. Then, the tangent matrix \mathbf{K}_{uu} of the displacement residual \mathbf{R}_u can be derived according to Eqs. (23), (24), and (27).

Considering the partial derivative of the Cauchy stress $\boldsymbol{\sigma}$ in Eq. (19) with respect to the chemical potential μ ,

$$\frac{\partial \boldsymbol{\sigma}}{\partial \mu} = \frac{\partial \boldsymbol{\sigma}}{\partial \lambda_s} \frac{d\lambda_s}{d\mu} + \frac{\partial \boldsymbol{\sigma}}{\partial \phi_d} \frac{d\phi_d}{d\mu} - \mathbf{I} \quad (32)$$

where

$$\begin{cases} \frac{\partial \boldsymbol{\sigma}}{\partial \phi_d} = \frac{G_d v}{J'' kT} \left(\frac{\mathbf{B}_d''}{\lambda_s} - \frac{\mathbf{I}}{\lambda_s^3} \right) - \frac{N_v}{J''} \left(\frac{\mathbf{B}_s''}{\lambda_s} - \frac{\mathbf{I}}{\lambda_s^3} \right) \\ \frac{d\phi_d}{d\mu} = - \frac{\exp \left(-\frac{\mu - \mu_r}{A} \right)}{A \left[1 + \exp \left(-\frac{\mu - \mu_r}{A} \right) \right]^2} \\ \frac{\partial \boldsymbol{\sigma}}{\partial \lambda_s} = \frac{\phi_d G_d v}{J'' kT} \left(-\frac{\mathbf{B}_d''}{\lambda_s^2} + \frac{3\mathbf{I}}{\lambda_s^4} \right) + \frac{\phi_s N_v}{J''} \left(-\frac{\mathbf{B}_s''}{\lambda_s} + \frac{3\mathbf{I}}{\lambda_s^3} \right) \\ \quad + \left(\frac{3}{J'' \lambda_s^4} - \frac{3}{J'' \lambda_s^4} - \frac{6\chi}{J''^2 \lambda_s^7} \right) \mathbf{I} \end{cases} \quad (33)$$

To identify the derivative of the free-swelling stretch λ_s with respect to chemical potential μ , the total differentiation is used for Eq. (15), and $d\lambda_s/d\mu$ can be obtained

$$\frac{d\lambda_s}{d\mu} = \frac{1 - \left(\frac{G_d v}{kT} - N_v \right) \left(\frac{1}{\lambda_s} - \frac{1}{\lambda_s^3} \right) \frac{d\phi_d}{d\mu}}{\left(\frac{G_d v}{kT} - N_v \right) \left(-\frac{1}{\lambda_s^2} + \frac{3}{\lambda_s^4} \right) + \frac{3}{\lambda_s^4} - \frac{3}{\lambda_s^4} - \frac{7\chi}{\lambda_s^7}} \quad (34)$$

Combining Eqs. (32)–(34), the tangent matrix \mathbf{K}_{uu} of the displacement residual \mathbf{R}_u can be determined. With the tangents matrix \mathbf{K}_{uu} and $\mathbf{K}_{\mu\mu}$ of the residual \mathbf{R}_μ , the water-triggered shape memory effects of hydrogels can be simulated by the FEM using the coding UEL.

4 Validation

In this section, three examples are utilized to validate the performance of the proposed model in describing the water-triggered shape memory effects of hydrogels. First, we applied uniaxial loading with different stretches on a block of hydrogel to validate

Table 1 Dimensionless parameters in the model for the simulation

Model parameters	Values
$\frac{G_d v}{kT}$	0.1
$\hat{\mu}_r$	-0.035
$\hat{\mu}_l$	-0.05
$\hat{\mu}_h$	-0.02
A	0.0015
l	0.98
Nv	0.001
χ	0.1

the accuracy of the UEL in describing the shape memory process and different shape recovery processes, including free-recovery and fixed-recovery conditions. Subsequently, the shape memory behaviors of a self-bending bilayer structure and a four-arm gripper are investigated by experiments, and the experiment results are compared with the predicted results by simulation. For the numerical examples below, the dimensionless parameters in the proposed model for simulation are listed in Table 1.

4.1 Validation Under Uniaxial Loading Condition. To validate the accuracy of the UEL, we simulated the constitutive relationships in the shape memory process of the hydrogel under uniaxial loading conditions, and we compared the FEM results with the analytical solutions. When the hydrogel is subjected to a uniaxial load, $F = \text{diag}(\lambda_1, \lambda_2, \lambda_3)$ and $\lambda_2 = \lambda_3$. Hence, the stress in the loading direction can be obtained using Eq. (21)

$$\frac{\sigma_1 v}{kT}(\lambda_1, \lambda_2, \mu) = \frac{\phi_d G_d v}{kT \lambda_1 \lambda_2^2} \left(\frac{\lambda_1^2}{\lambda_{f1}^2} - 1 \right) + \frac{\phi_s N v}{\lambda_1 \lambda_2^2} (\lambda_1^2 - 1) + \left(\log \left(1 - \frac{1}{\lambda_1 \lambda_2^2} \right) + \frac{1}{\lambda_1 \lambda_2^2} + \frac{\chi}{\lambda_1^2 \lambda_2^4} - \frac{\mu}{kT} \right) \quad (35)$$

The stresses in the transverse direction vanish, i.e., $\sigma_2 = \sigma_3 = 0$; hence,

$$\frac{\phi_d G_d v}{kT} \left(\frac{\lambda_2^2}{\lambda_{f2}^2} - 1 \right) + \phi_s N v (\lambda_2^2 - 1) + \lambda_1 \lambda_2^2 \left(\log \left(1 - \frac{1}{\lambda_1 \lambda_2^2} \right) + \frac{1}{\lambda_1 \lambda_2^2} + \frac{\chi}{\lambda_1^2 \lambda_2^4} - \frac{\mu}{kT} \right) = 0 \quad (36)$$

This equation determines the transverse stretch λ_2 for a given loading stretch λ_1 . The frozen stretches λ_{f1} and λ_{f2} can be determined using Eq. (2). Together with Eqs. (35) and (36), the constitutive relationship of water-triggered SMHs in the shape memory cycle under uniaxial loading conditions can be obtained analytically.

Three types of shape recovery processes of water-triggered shape memory hydrogels are investigated: the free-recovery process, fixed-recovery process 1, and fixed-recovery process 2, as shown in Fig. 3. To better understand the constitutive relationship of $\sigma - \lambda - \hat{\mu}$, three schematics of the corresponding shape memory cycles are shown in Figs. 4(a)–4(c). The shape memory process can be divided into three processes. In the first process ①, a mechanical load is applied to the hydrogel at a high chemical potential $\hat{\mu}_h$ from the initial state “A” to a state of pre-programmed “B.” The second process ② is the constrained dehydration process. The hydrogel is dehydrated to a low chemical potential $\hat{\mu}_l$ (state “C”) with the pre-stretch λ_{pre} maintained. Followed by the unloading process (the third process ③), the mechanical constraint is removed from the specimen at the chemical potential $\hat{\mu}_l$ from state “C” to state “D.” These first three processes are called programming process, i.e., the shape programmed at high chemical potential $\hat{\mu}_h$ is memorized as a temporary shape at a low chemical potential $\hat{\mu}_l$ with a stable condition.

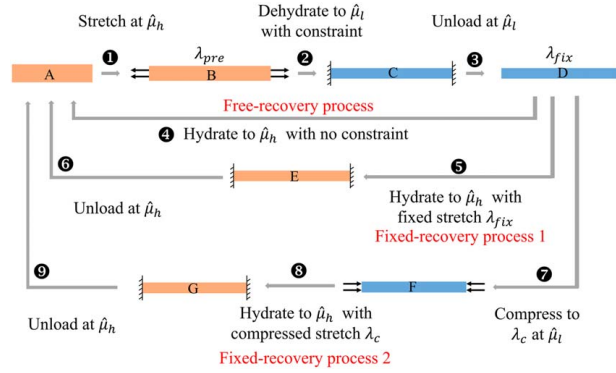


Fig. 3 Schematics of three types of shape memory cycles of water-trigger shape memory effects, including free-recovery process, fixed-recovery process 1, and fixed-recovery process 2

When hydrating the specimen to chemical potential $\hat{\mu}_h$ with no constraint, the memorized shape can be recovered from the temporary shape (state “D”) to the initial shape (state “A”); this process is called the free-recovery process (④ in Fig. 3). To explore the stress response of the hydrogel under external constraints during the recovery process, two fixed-recovery processes are investigated. As shown in Fig. 3, the fixed-recovery process 1 is to hydrate the

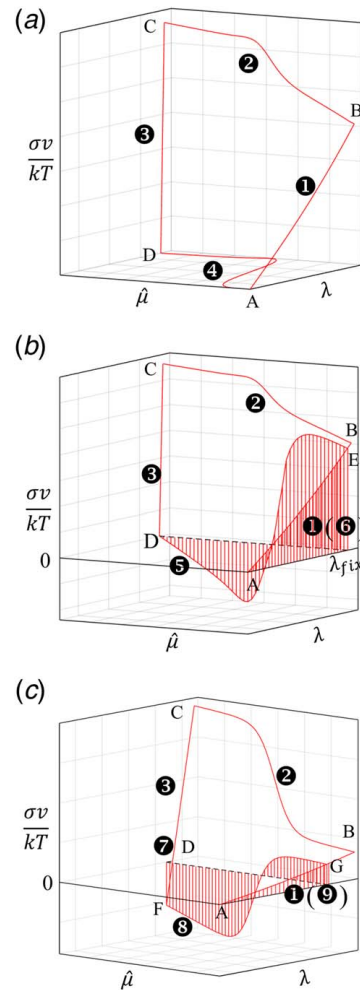


Fig. 4 General schematics of the stress-stretch-normalized chemical potential ($\sigma - \lambda - \hat{\mu}$) relationship for (a) free-recovery process, (b) fixed-recovery process 1, and (c) fixed-recovery process 2

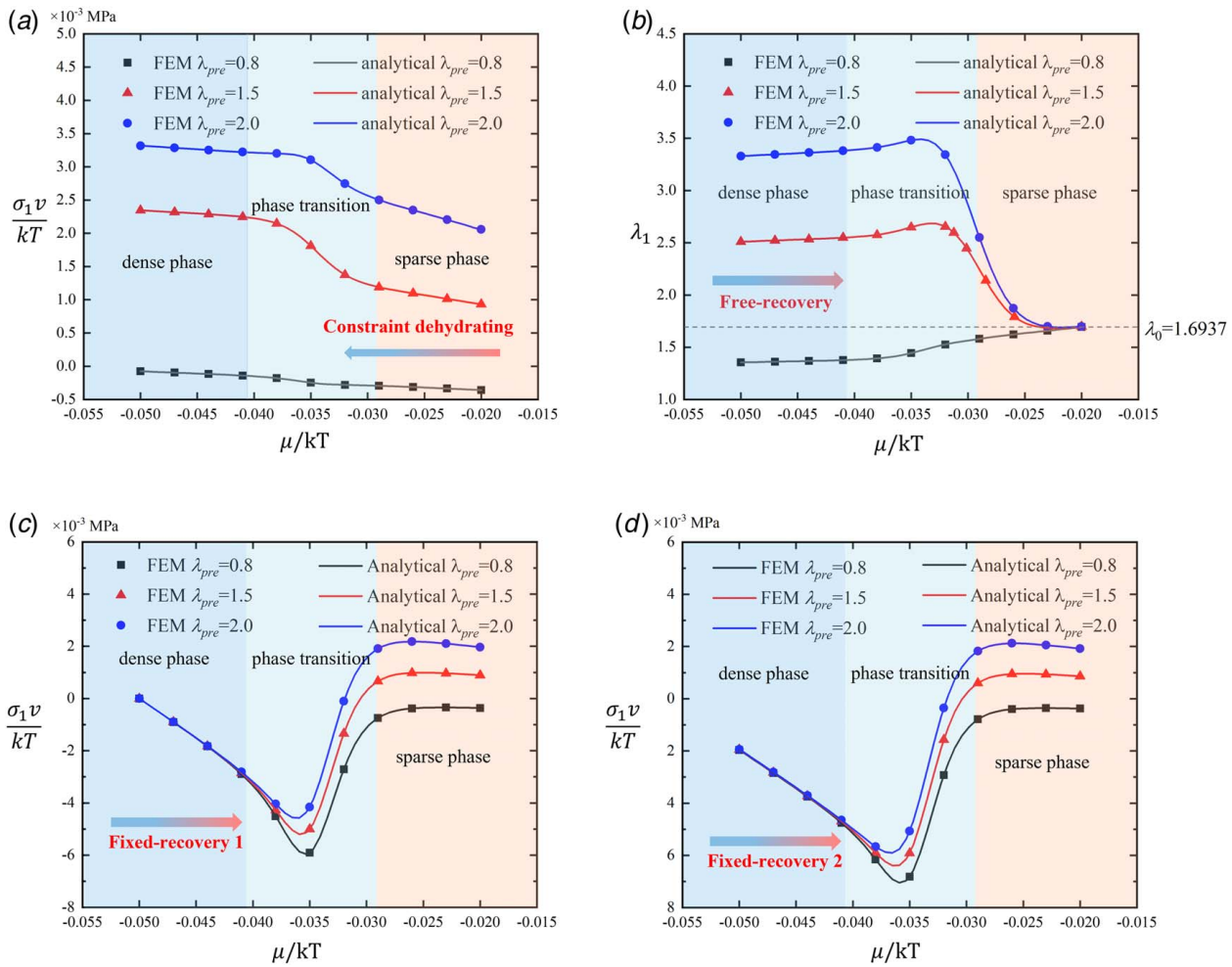


Fig. 5 Validation of the accuracy of the FEM implementation by comparing with analytical results in different processes: (a) stress–chemical potential relationship in the constraint-dehydrating process; (b) stretch–chemical potential relationship in the free-recovery process; (c) stress–chemical potential relationship in the fixed-recovery process 1, and (d) fixed-recovery process 2

temporary shape from $\hat{\mu}_l$ to $\hat{\mu}_h$ with fixed stretch λ_{fix} , and the hydrogel reaches state “E.” After unloading the constraint in the hydrogel, the deformation can be full recovery to the initial state “A.” In fixed-recovery process 2, the temporary shape is compressed to λ_c (state “F”) at $\hat{\mu}_l$ and then hydrated to $\hat{\mu}_h$ (state “G”) with the compressed stretched λ_c . Followed by unloading the constraint in state “G,” the compressed stretched λ_c can be fully recovered.

To validate the accuracy of the finite-element implementation of the proposed model, we investigate the constitutive relationship in constrained dehydrating process (process v in Fig. 3), free-recovery process (process x in Fig. 3 and Fig. 4(a)), fixed-recovery process 1 (process 5 in Fig. 3 and Fig. 4(b)), and fixed-recovery process 2

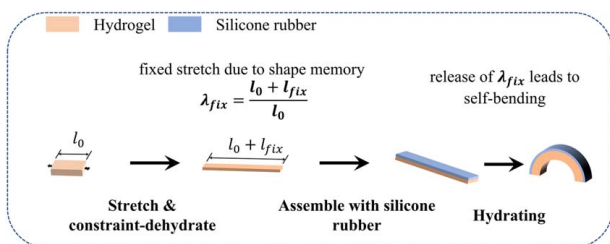


Fig. 6 Schematic of a self-bending bilayer structure

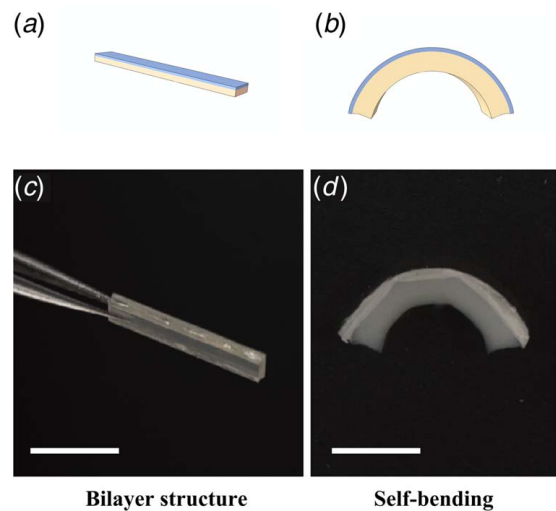


Fig. 7 Comparison of simulation and experimental results of a self-bending bilayer structure. Simulated results: (a) and (b); experimental results: (c) and (d). The bilayer structure ((a) and (c)) will bend itself into an arch ((c) and (d)) when hydrating. The scale bar is 1.0 cm.

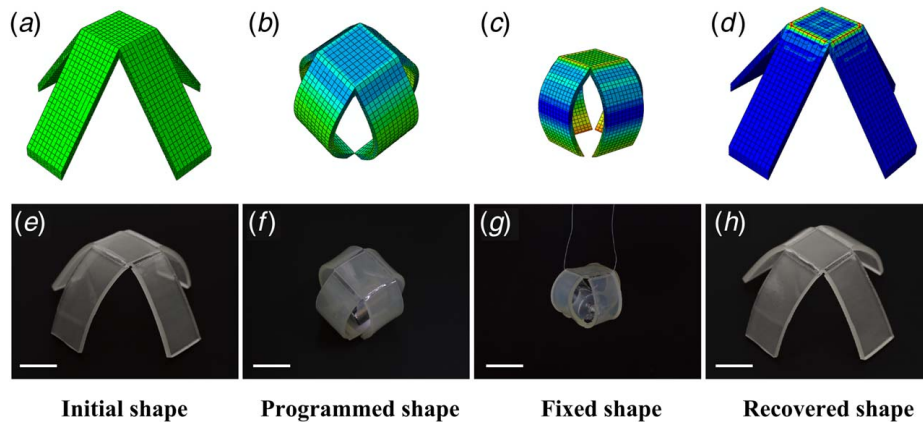


Fig. 8 Simulated and experimental results of a gripper structure during the shape memory cycle for water-triggered SMH, (a)—(d) simulated results; (e)—(f) experimental results. (a) and (e) initial shape at high water content; (b) and (f) programmed shape at high water content; (c) and (g) fixed shape at low water content; (d) and (h) recovered shape at high water content. The scale bar is 1.0 cm.

(process ③ in Fig. 3 and Fig. 4(c)) of a block of hydrogel. We simulate the uniaxial loading condition with different pre-stretches, $\lambda_{pre} = 0.8, 1.5, 2.0$, in which $\lambda_{pre} = 0.8$ refers to compression condition. The compress stretch is set by the equation $\lambda_c/\lambda_{fix} = 1\%$. The comparison between the FEM results and the analytical solutions is shown in Fig. 5. The relationship between the stress σ_1 and the chemical potential μ/kT in the constrained dehydrating process is shown in Fig. 5(a). It can be seen that the stress increased as the chemical potential decreases, and the stress undergoes three stages. While the hydrogel is in the sparse or dense phase, the stress in the constraint-dehydrating process did not increase significantly. When the hydrogel goes through the phase transition, the stress has a significant increase owing to the sharp change in the modulus of hydrogel during the phase transition. Figure 5(b) shows the relationship between the stretch λ_1 and the chemical potential μ/kT in the free-recovery process with the stress-free condition. At the beginning of the hydrating process, the stretch has increased slightly because of the swelling properties of the hydrogel. When the chemical potential crosses the central point of the phase transition, the memorized stretches are gradually released to the initial state. The relationships between σ_1 and μ/kT in two fixed-recovery processes are shown in Figs. 5(c) and 5(d), respectively. At the beginning of the hydrating process, the stress gradually decreases in a compression mode owing to swelling under a stretch constraint (λ_{fix} or λ_c). When the chemical potential approaches the central point of the phase transition, the stress reaches its peak value and then gradually increases. As the hydrogel completes its transformation from the dense phase to the sparse phase, the stress tends to a plateau state. The stress and stretch responses during shape memory cycles indicate that the proposed model has a good performance in describing the entire shape memory process of water-triggered SMHs. Additionally, the analytical stress responses and stretches responses in different shape memory cycles have a good agreement with that of FEM results. The good consistency validates the accuracy of the UEL subroutine in describing the water-triggered shape memory behaviors.

4.2 Experimental Validation. In this section, we compare the corresponding experimental results with the simulation predictions of the water-triggered shape memory behaviors of the two structures. First, an acrylamide aqueous solution is prepared using the standard method [42]. Subsequently, the precursor solution of PAAm hydrogel is molded into a strip and a 3D four-arm gripper structure. A strip is prepared for the bilayer structure. The synthesized samples are used in the experiment as the water-triggered SMHs.

We first conduct an experiment of a self-bending bilayer structure consisting of two layers, an active layer and a passive layer. As

shown in Fig. 6, the hydrogel with initial shape is first stretched at a high water content and then dehydrated to a low water content under constraint. After unloading, a strip of hydrogel with a fixed stretch λ_{fix} is obtained and acts as an active layer. Subsequently, the hydrogel strip is assembled with silicone rubber, which acts as a passive layer. When hydrating the two layers, the fixed stretch of the active layer is released whereas the passive rubber does not deform. As a result of the mismatch between the two layers during hydration, the bilayer structure will bend itself. The experimental results for the self-bending bilayer are shown in Figs. 7(c) and 7(d). To verify the prediction ability of the proposed model, we simulated the self-bending process via the FEM using the coded UEL, and the results are shown in Figs. 7(a) and 7(b). A comparison between the simulation and experimental results is shown in Fig. 7. The good agreement with the self-bending shape of the bilayer structure indicates that the proposed model can effectively describe the water-triggered shape recovery process of the hydrogel.

To further verify the effectiveness of the model in describing the shape memory behaviors, the grabbing and releasing process of a gripper structure is investigated through experiments and simulations. The simulation and experimental results are shown in Figs. 8(a)–8(f), respectively. To obtain the temporary shape, we first bend the four arms of the gripper (Fig. 8(b)) at a high chemical potential, $\hat{\mu}_h$. Subsequently, the chemical potential of the programmed shape reduces to a low chemical potential, $\hat{\mu}_l$, under the constraint. After the constraints are removed, a fixed shape can be obtained as shown in Fig. 8(c). It can be seen that the gripper can hold a weight of 50 g in the fixed shape state (Fig. 8(g)). Finally, the fixed shape recovers to its initial shape (Fig. 8(d)) after the chemical potential is increased to high chemical potential, $\hat{\mu}_h$, and the weight is released as the water content of the gripper increases (Fig. 8(h)). Through a comparison of different shapes during the shape memory cycle between simulations and experiments (Fig. 8), good consistency verifies the model can predict the water-triggered shape memory behaviors of hydrogels under complex deformation.

5 Conclusions

In this study, a thermodynamic constitutive model for water-triggered SMHs is developed based on the assumption that the hydrogel is a mixture of dense and sparse phases. In the proposed model, two internal state variables are used to describe the shape memory effects. The first internal state variable is the frozen deformation gradient used to investigate the stored and released deformations in shape memory and shape recovery process, respectively.

The second internal state variable is the volume fraction of the dense phase during the phase transition, which quantifies the degree of the phase transition owing to hydration and dehydration. For verification, the proposed model is implemented into FEM using a user-defined subroutine UEL in ABAQUS. In the UEL subroutine, the deformation gradient is decomposed by separating the swelling and mechanical deformations to capture the swelling stretch at the reference configuration which is a swollen state. Utilizing the coded UEL subroutine, several examples are simulated to verify the performance of the model in describing the water-triggered shape memory behavior of hydrogels. First, the constitutive relationships of the shape memory process and three different shape recovery processes under three uniaxial loads ($\lambda_{pre} = 0.8, 1.5, 2.0$) are simulated, and the consistency between the analytical and simulated results validates the accuracy of the finite-element implementation. In addition, the shape memory behaviors of a self-bending bilayer structure and a four-arm gripper are investigated by comparing the experimental results with the simulated results. The good consistency between the simulation and experiment validates the efficiency of the proposed model in predicting the water-triggered shape memory effects of hydrogels. The results of this study provide researchers with a theoretical model to investigate the mechanical behaviors of water-triggered shape memory hydrogels and a tool for designing and optimizing new structures based on SMHs.

Acknowledgment

The authors are grateful for the support from the National Natural Science Foundation of China (Grant Nos. 11820101001 and 12172273).

Conflict of Interest

There are no conflicts of interest.

Data Availability Statement

The data sets generated and supporting the findings of this article are obtainable from the corresponding author upon reasonable request.

References

- Cui, Y., Tan, M., Zhu, A., and Guo, M., 2014, "Mechanically Strong and Stretchable PEG-Based Supramolecular Hydrogel With Water-Responsive Shape-Memory Property," *J. Mater. Chem. B*, **2**(20), pp. 2978–2982.
- Zhang, J. L., Huang, W. M., Gao, G., Fu, J., Zhou, Y., Salvekar, A. V., Venkatraman, S. S., Wong, Y. S., Tay, K. H., and Birch, W. R., 2014, "Shape Memory/Change Effect in a Double Network Nanocomposite Tough Hydrogel," *Eur. Polym. J.*, **58**, pp. 41–51.
- Liu, Y., Li, Y., Chen, H., Yang, G., Zheng, X., and Zhou, S., 2014, "Water-Induced Shape-Memory Poly (d, l-Lactide)/Microcrystalline Cellulose Composites," *Carbohydr. Polym.*, **104**, pp. 101–108.
- Chen, C., Lei, J., and Liu, Z., 2022, "A Ternary Seismic Metamaterial for Low Frequency Vibration Attenuation," *Materials*, **15**(3), p. 1246.
- Chen, Y., Yin, L., Ge, F., Tong, X., Zhang, H., and Zhao, Y., 2021, "Liquid Crystalline Hydrogel With Thermally Induced Reversible Shape Change and Water-Triggered Shape Memory," *Macromol. Rapid Commun.*, **42**(23), p. 2100495.
- Falqi, F. H., Bin-Dahman, O. A., Khair, A., and Al-Harthi, M. A., 2022, "PVA/PEG/Graphene Shape Memory Composites Responsive to Multi-Stimuli," *Appl. Phys. A*, **128**(5), pp. 1–11.
- Huang, J., Zhao, L., Wang, T., Sun, W., and Tong, Z., 2016, "NIR-Triggered Rapid Shape Memory PAM-GO-Gelatin Hydrogels With High Mechanical Strength," *ACS Appl. Mater. Interfaces*, **8**(19), pp. 12384–12392.
- Chen, Y., Liu, T., Wang, G., Liu, J., Zhao, L., Zhang, R., and Yu, Y., 2021, "Intelligent Response Bilayer Hydrogel With Controllable Deformation-Recovery and Shape Memory," *Eur. Polym. J.*, **150**, p. 110399.
- Gong, X.-L., Xiao, Y.-Y., Pan, M., Kang, Y., Li, B.-J., and Zhang, S., 2016, "pH- and Thermal-Responsive Multishape Memory Hydrogel," *ACS Appl. Mater. Interfaces*, **8**(41), pp. 27432–27437.
- Hu, Q., Zhang, Y., Wang, T., Sun, W., and Tong, Z., 2021, "pH Responsive Strong Polyion Complex Shape Memory Hydrogel With Spontaneous Shape Changing and Information Encryption," *Macromol. Rapid Commun.*, **42**(9), p. 2000747.
- Ma, Y., Hua, M., Wu, S., Du, Y., Pei, X., Zhu, X., Zhou, F., and He, X., 2020, "Bioinspired High-Power-Density Strong Contractile Hydrogel by Programmable Elastic Recoil," *Sci. Adv.*, **6**(47), p. eabd2520.
- Cui, Y., Li, D., Gong, C., and Chang, C., 2021, "Bioinspired Shape Memory Hydrogel Artificial Muscles Driven by Solvents," *ACS Nano*, **15**(8), pp. 13712–13720.
- Li, Z., Cai, J., Wei, M., and Chen, J., 2022, "An UV-Photo and Ionic Dual Responsive Interpenetrating Network Hydrogel With Shape Memory and Self-Healing Properties," *RSC Adv.*, **12**(24), pp. 15105–15114.
- Liang, Y., Shen, Y., and Liang, H., 2022, "Solvent-Responsive Strong Hydrogel With Programmable Deformation and Reversible Shape Memory for Load-Carrying Soft Robot," *Mater. Today Commun.*, **30**, p. 103067.
- Zhao, Z., Zhang, K., Liu, Y., Zhou, J., and Liu, M., 2017, "Highly Stretchable, Shape Memory Organohydrogels Using Phase-Transition Microinclusions," *Adv. Mater.*, **29**(33), p. 1701695.
- Liu, K., Zhang, Y., Cao, H., Liu, H., Geng, Y., Yuan, W., Zhou, J., Wu, Z. L., Shan, G., and Bao, Y., 2020, "Programmable Reversible Shape Transformation of Hydrogels Based on Transient Structural Anisotropy," *Adv. Mater.*, **32**(28), p. 2001693.
- Fan, W., Zhang, Z., Liu, Y., Wang, J., Li, Z., and Wang, M., 2021, "Shape Memory Polyacrylamide/Gelatin Hydrogel With Controllable Mechanical and Drug Release Properties Potential for Wound Dressing Application," *Polymer*, **226**, p. 123786.
- Korde, J. M., and Kandasubramanian, B., 2020, "Naturally Biomimicked Smart Shape Memory Hydrogels for Biomedical Functions," *Chem. Eng. J.*, **379**, p. 122430.
- Zhang, Y., Liu, K., Liu, T., Ni, C., Chen, D., Guo, J., Liu, C., Zhou, J., Jia, Z., and Zhao, Q., 2021, "Differential Diffusion Driven Far-From-Equilibrium Shape-Shifting of Hydrogels," *Nat. Commun.*, **12**(1), pp. 1–8.
- Zhu, C. N., Bai, T., Wang, H., Ling, J., Huang, F., Hong, W., Zheng, Q., and Wu, Z. L., 2021, "Dual-Encryption in a Shape-Memory Hydrogel With Tunable Fluorescence and Reconfigurable Architecture," *Adv. Mater.*, **33**(29), p. 2102023.
- Qiao, L., Liu, C., Liu, C., Zong, L., Gu, H., Wang, C., and Jian, X., 2022, "Self-Healing, pH-Sensitive and Shape Memory Hydrogels Based on Acylhydrazone and Hydrogen Bonds," *Eur. Polym. J.*, **162**, p. 110838.
- Chen, Y., Zhang, H., Chen, J., Kang, G., and Hu, Y., 2021, "Hyperelastic Model for Polyacrylamide-Gelatin Double Network Shape-Memory Hydrogels," *Acta Mech. Sin.*, **37**(5), pp. 748–756.
- Lu, H., Li, Z., Wang, X., Xing, Z., and Fu, Y. Q., 2021, "Negatively Thermodynamic Toughening in Double Network Hydrogel Towards Cooling-Triggered Multi-Shape Memory Effect," *Smart Mater. Struct.*, **30**(10), p. 105011.
- Tobushi, H., Hashimoto, T., Hayashi, S., and Yamada, E., 1997, "Thermomechanical Constitutive Modeling in Shape Memory Polymer of Polyurethane Series," *J. Intell. Mater. Syst. Struct.*, **8**(8), pp. 711–718.
- Li, Y., Hu, J., and Liu, Z., 2017, "A Constitutive Model of Shape Memory Polymers Based on Glass Transition and the Concept of Frozen Strain Release Rate," *Int. J. Solids Struct.*, **124**, pp. 252–263.
- Huang, R., Zheng, S., Liu, Z., and Ng, T. Y., 2020, "Recent Advances of the Constitutive Models of Smart Materials—Hydrogels and Shape Memory Polymers," *Int. J. Appl. Mech.*, **12**(02), p. 2050014.
- Li, Y., He, Y., and Liu, Z., 2017, "A Viscoelastic Constitutive Model for Shape Memory Polymers Based on Multiplicative Decompositions of the Deformation Gradient," *Int. J. Plast.*, **91**, pp. 300–317.
- Li, Y., and Liu, Z., 2018, "A Novel Constitutive Model of Shape Memory Polymers Combining Phase Transition and Viscoelasticity," *Polymer*, **143**, pp. 298–308.
- Xue, Y., Lei, J., and Liu, Z., 2022, "A Thermodynamic Constitutive Model for Shape Memory Polymers Based on Phase Transition," *Polymer*, **243**, p. 124623.
- Liu, Y., Gall, K., Dunn, M. L., Greenberg, A. R., and Diani, J., 2006, "Thermomechanics of Shape Memory Polymers: Uniaxial Experiments and Constitutive Modeling," *Int. J. Plast.*, **22**(2), pp. 279–313.
- Hong, W., Liu, Z., and Suo, Z., 2009, "Inhomogeneous Swelling of a Gel in Equilibrium With a Solvent and Mechanical Load," *Int. J. Solids Struct.*, **46**(17), pp. 3282–3289.
- Ding, Z., Toh, W., Hu, J., Liu, Z., and Ng, T. Y., 2016, "A Simplified Coupled Thermo-Mechanical Model for the Transient Analysis of Temperature-Sensitive Hydrogels," *Mech. Mater.*, **97**, pp. 212–227.
- Miehe, C., 1996, "Numerical Computation of Algorithmic (Consistent) Tangent Moduli in Large-Strain Computational Inelasticity," *Comput. Methods Appl. Mech. Eng.*, **134**(3–4), pp. 223–240.
- Sun, W., Chaikof, E. L., and Levenston, M. E., 2008, "Numerical Approximation of Tangent Moduli for Finite Element Implementations of Nonlinear Hyperelastic Material Models," *ASME J. Biomech. Eng.*, **130**(6), p. 061003.
- Chester, S. A., Di Leo, C. V., and Anand, L., 2015, "A Finite Element Implementation of a Coupled Diffusion-Deformation Theory for Elastomeric Gels," *Int. J. Solids Struct.*, **52**, pp. 1–18.
- Narayan, S., and Anand, L., 2022, "A Coupled Electro-Chemo-Mechanical Theory for Polyelectrolyte Gels With Application to Modeling Their Chemical Stimuli-Driven Swelling Response," *J. Mech. Phys. Solids*, **159**, p. 104734.
- Kumbhar, P., Swaminathan, N., and Annabattula, R. K., 2022, "Mesoscale Analysis of Li-Ion Battery Microstructure Using Sequential Coupling of

- Discrete Element and Finite Element Method,” *Int. J. Energy Res.*, **46**(9), pp. 12003–12025.
- [38] Qi, H. J., Nguyen, T. D., Castro, F., Yakacki, C. M., and Shandas, R., 2008, “Finite Deformation Thermo-Mechanical Behavior of Thermally Induced Shape Memory Polymers,” *J. Mech. Phys. Solids*, **56**(5), pp. 1730–1751.
- [39] Hong, W., Zhao, X., Zhou, J., and Suo, Z., 2008, “A Theory of Coupled Diffusion and Large Deformation in Polymeric Gels,” *J. Mech. Phys. Solids*, **56**(5), pp. 1779–1793.
- [40] Ding, Z., Liu, Z., Hu, J., Swaddiwudhipong, S., and Yang, Z., 2013, “Inhomogeneous Large Deformation Study of Temperature-Sensitive Hydrogel,” *Int. J. Solids Struct.*, **50**(16–17), pp. 2610–2619.
- [41] Xu, S., and Liu, Z., 2019, “A Nonequilibrium Thermodynamics Approach to the Transient Properties of Hydrogels,” *J. Mech. Phys. Solids*, **127**, pp. 94–110.
- [42] Li, Z., Liu, Z., Ng, T. Y., and Sharma, P., 2020, “The Effect of Water Content on the Elastic Modulus and Fracture Energy of Hydrogel,” *Extreme Mech. Lett.*, **35**, p. 100617.